Available online at www.sciencedirect.com
SCIENCE DIRECT®
Journal of Sound and Vibration 293 (2006) 125–137
JOURNAL OF SOUND AND VIBRATION
www.elsevier.com/locate/jsvi

The development of a dynamic amplification estimator for bridges with good road profiles

Yingyan Li*, Eugene OBrien, Arturo González

School of Architecture, Landscape & Civil Engineering, University College Dublin, Earlsfort Terrace, Dublin 2, Ireland

Received 2 February 2005; received in revised form 8 September 2005; accepted 22 September 2005
Available online 10 November 2005

Abstract

The paper considers the influence of the surface profile on the dynamic amplification of a simply supported bridge when subject to a quarter-car vehicle model. The effect of the profile irregularities on the bridge dynamic amplification is characterized with a 'response surface' giving dynamic amplification due to a 'unit ramp' at any location. Even though the dynamic interaction problem is nonlinear, the effects of all ramps which together make up a road profile can be calculated separately and added using the 'response surface'. This superposition process achieves reasonable accuracy for 'good' (moderately smooth) surface profiles. An accurate estimate of dynamic amplification for bridges is demonstrated with a wide range of good profiles.
© 2005 Elsevier Ltd. All rights reserved.

1. Introduction

Dynamic amplification can have a significant effect on the stresses in a bridge, particularly when its natural frequency is excited by vehicles traveling at speeds which induce a resonance effect. The dynamic amplification factor (DAF) is defined as the ratio of the maximum total (static plus dynamic) response of the bridge to the maximum static response. The draft Eurocode for Bridge Loading [1] assumes impact factors to be a function of span length. However, the interaction between bridge, truck and road roughness is known to involve many parameters which are difficult to allow for when attempting to predict the bridge response [2]. Authors such as Olsson [3], Liu et al. [4] and Brady and OBrien [5] found the bridge's DAF to be significantly affected by the velocity of the vehicle and Green et al. [6] suggest that maximum amplification factors occur at different vehicle velocities for different bridges. Based on the work of Frýba [7], Brady et al. [8] carried out an extensive analysis of the effect on bridge response of a constant force traversing a beam at constant velocity. They showed that the DAF of a bridge with a smooth surface is highly dependent on the velocity of the vehicle.

Many other authors, using both experimental tests and complex numerical models, have examined the effect of parameters of the vehicle–bridge interaction system on a highway bridge's dynamic amplification. Authors such as Huang et al. [9], Zhu and Law [10], Michaltsos et al. [11] and DIVINE [2] find the effect of the weight of the vehicle and the number of vehicles on the DAF. Active and semi-active dampers in the vehicle are

*Corresponding author. Tel.: +353 1 716 7281; fax: +353 1 716 7299.
E-mail address: yingyan.li@ucd.ie (Y. Li).

0022-460X/$ - see front matter © 2005 Elsevier Ltd. All rights reserved.
doi:10.1016/j.jsv.2005.09.015

Nomenclature

C	passive damping coefficient of the vehicle model
c	constant speed of the interaction model
DAE	estimator of DAF
DAF	dynamic amplification factor
$\mathrm{DAF}^{\mathrm{smooth}}$	DAF for a smooth profile
$\mathrm{DAF}^{\mathrm{unit}}$	DAF for a unit ramp
E	Young's modulus of beam
f_1	first natural frequency of the bridge
g	acceleration due to gravity
h_u	height of unit ramp
i	number of intervals
J	second moment of area of beam cross-section
j	mode number
K_s	suspension stiffness of the vehicle model
K_t	tire stiffness of the vehicle model
l	beam length
$M(\xi,\tau)$	dimensionless bending moment
$M_R(\xi,\tau)$	dimensionless bending moment due to interaction force
$M_\mu(\xi,\tau)$	dimensionless bending moment due to bridge vibration
M_0	maximum static mid-span bending moment
m_s	sprung mass of the vehicle
m_t	unsprung mass of the vehicle
N	number of intervals/ramps
$q_{(j)}(\tau)$	normalized deflection for mode j and instant τ
$R(t)$	tire force imparted to the bridge at instant t
$\bar{R}(\tau)$	normalized interaction force
$r(x)$	road elevation at location x
$s(i)$	ramp scale factor for two adjacent measurement points
t	time ($t=0$ when the vehicle is located at the start of the bridge)
$v(x,t)$	deflection of the beam at position x and instant t
v_0	maximum mid-span static deflection
x	distance along the bridge ($x=0$ when the vehicle is located at the start of the bridge)
$y_s(t)$	vertical displacement of sprung mass at instant t
$y_t(t)$	vertical displacement of unsprung mass at instant t
α	speed parameter given by $c/(2f_1 l)$
$\delta(x)$	Dirac function (impulse, also known as delta function)
ε	parameter indicating whether the vehicle is on ($\varepsilon=1$) or off ($\varepsilon=0$) the bridge
μ	mass per unit length of the bridge
ξ	normalized distance along the bridge
τ	normalized time
ω_b	circular damping frequency of the beam
ω_n	frequency of the sprung mass

studied by Karnopp et al. [12], initially with the goal of reducing magnitudes of sprung mass accelerations. Semi-active suspension control strategies have been presented by Cebon [13] and Valášek et al. [14] with the goal of minimizing tire–pavement interaction forces as well as maintaining or improving vehicle ride quality.

Although many studies have given valuable quantitative information on dynamic amplification, they give little insight into how the amplification is affected by the roughness features of the bridge surface, which is a key component of the interaction system. Some authors such as Green et al. [6], Coussy et al. [15] and Liu et al. [4] have made allowance for the effect of roughness but have not considered it in detail. Many authors generate road profiles using a Gaussian random process which has the same spectral properties as those measured but does not distinguish between profiles where the locations of individual irregularities may be different. Kou and DeWolf [16] and Lei and Noda [17] allow for bridge surface profile in this way. In both of these papers, the influence of roughness is considered but the profile is made rougher by a simple scaling of a smoother profile. Chatterjee et al. [18] calculate the mean and standard deviation of dynamic amplification from 10 randomly generated profiles. Michaltsos [19] recognizes the importance of irregularity location on the bridge and highlights some locations where an irregularity can be important. Pesterev et al. [20,21] consider the contact forces acting on a pavement after a vehicle passes over an isolated road surface irregularity. Analytical solutions are derived for multi-degree-of-freedom vehicles crossing different irregularity functions. While this work focuses on surface contact forces, it is pointed out that a similar approach is applicable to

bridges. Mikaltsos and Konstantakopoulos [22] consider the influence of a single bump at a number of discrete locations on bridge dynamics. The size and shape are considered and the inaccuracies that result when two uni-axial models are used to approximate a 2-axle model. There is no consideration given in the above references to the superposition of the effects of multiple irregularities.

A road profile can contribute significantly to vehicle dynamics leading to substantial increases in the bridge load effect. This paper considers the influence of unit 'ramps' and full road profiles on bridge dynamic amplification. Simulations are based on the interaction of a quarter-car model and a Bernoulli–Euler beam. Only the road profile and the speed are varied. A number of road profiles are considered, all classified as 'good' according to the ISO standard. A 'good' profile is defined as one with an International Roughness Index (IRI) lower than 7 m/km [23]. It is shown that dynamic amplification can be reasonably accurately predicted by superposing the DAFs due to each ramp that makes up the profile. This is a finding of great importance for a number of reasons. The calculation of DAF normally involves the solution of complex differential equations whereas estimation by superposition is computationally trivial. Estimates of dynamic amplification found in this way can be used as a measure of road roughness as it relates to bridge stress which is far more useful than any existing measure such an International Roughness Index. Finally, the bridge dynamic response to unit ramps provides a means by which Engineers and students can understand the factors that contribute to dynamic amplification.

2. Vehicle–bridge interaction model

A quarter-car is used to model the vehicle (Fig. 1). It is represented as a two-degree-of-freedom suspension system traveling at constant velocity, c, over a simply supported Bernoulli–Euler beam with constant cross section and mass per unit length. A typical beam-and-slab construction with precast concrete Y-beams [24,25] was assumed to calculate a representative mass per meter, μ, and second moment of area, J.

The equations of motion controlling this system are given by ordinary differential equations (1a) and (1b) [7]. The sprung mass of the vehicle, m_s, has a vertical body displacement $y_s(t)$, while the unsprung mass, m_t, has vertical axle displacement $y_t(t)$.

$$-m_s \frac{d^2 y_s(t)}{dt^2} - K_s[y_s(t) - y_t(t)] - C\left[\frac{dy_s(t)}{dt} - \frac{dy_t(t)}{dt}\right] = 0, \tag{1a}$$

$$(m_t + m_s)g - m_t \frac{d^2 y_t(t)}{dt^2} + K_s[y_s(t) - y_t(t)] + C\left[\frac{dy_s(t)}{dt} - \frac{dy_t(t)}{dt}\right] - R(t) = 0, \tag{1b}$$

where $R(t)$ is the tire force imparted to the bridge, given by Eq. (2). In the numerical model, the tire force is prevented from becoming negative, because the tire is incapable of applying a suction to the bridge surface.

$$R(t) = K_t[y_t(t) - v(x_1, t) - r(x_1)] \geqslant 0. \tag{2}$$

The deflection $v(x_1,t)$ is the instantaneous deflection of the beam underneath the vehicle at position $x_1 = ct$, while $r(x_1)$ is the surface roughness at the position of the vehicle. Linear quantities K_s and K_t describe the

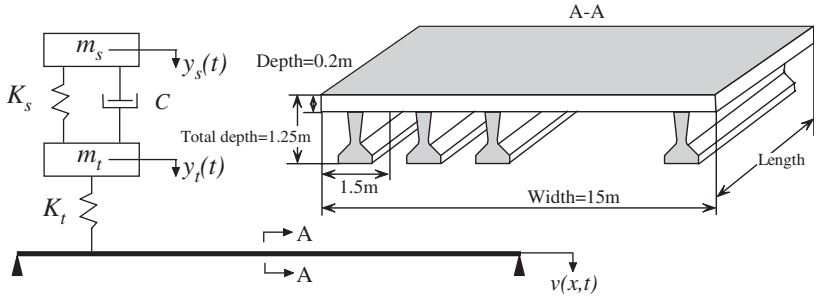

Fig. 1. Schematic of the vehicle and bridge cross-section.

Table 1
Vehicle and beam properties

Vehicle properties			Beam properties		
Physical description	Symbol	Value	Physical description	*Symbol*	Value
Sprung mass	m_s	9000 kg	Mass per unit length	μ	18358 kg/m
Unsprung mass	m_t	1000 kg	Second moment of area of beam cross-section	J	1.3901 m^4
Suspension stiffness	K_s	80 kN/m	Bridge length	l	25 m
Tire vertical stiffness	K_t	1800 kN/m	Young's modulus of beam	E	3.5×10^{10} N/m^2
Passive damping coefficient	C	7 kN s/m			

vertical stiffness of the suspension spring and tire, respectively. A full list of beam and vehicle parameters (representative of a typical air sprung suspension) is given in Table 1 [26,27].

The beam deflection is given by the solution of Eq. (3), the governing Bernoulli–Euler equation:

$$EJ\frac{\partial^4 v(x,t)}{\partial x^4}+\mu\frac{\partial^2 v(x,t)}{\partial t^2}+2\mu\omega_b\frac{\partial v(x,t)}{\partial t}=\delta(x-ct)R(t). \tag{3}$$

Numerical results are determined in the domain $0\leqslant x\leqslant l$, $0\leqslant t\leqslant l/c$. The Dirac function, $\delta(x-ct)$, ensures that the vehicle–bridge interaction force is only applied in this domain. In order to facilitate comparison of beam deflections across a wide range of velocities, a normalized deflection, $q_{(j)}(\tau)$, for each mode of vibration, j, of the bridge is calculated in the normalized domains $0\leqslant\xi\leqslant 1$ and $0\leqslant\tau\leqslant 1$, where $\xi=x/l$ and $\tau=ct/l$. This is expressed as

$$v(x,t)=v_0\sum_{j=1}^{\infty}q_{(j)}(\tau)\sin\frac{j\pi ct}{l}, \tag{4}$$

where v_0 is the corresponding mid-span static deflection, given by

$$v_0=\frac{2(m_t+m_s)gl^3}{\pi^4 EJ}. \tag{5}$$

The bridge DAF is the maximum total mid-span bending moment, normalized through division by its static equivalent, $M_0=(m_t+m_s)gl/4$. The normalized bending moment at mid-span can also be calculated by the sum of the normalized interaction force bending and the bridge dynamic bending components, which is expressed by [7]

$$M(\xi,\tau)=M_R(\xi,\tau)+M_\mu(\xi,\tau), \tag{6}$$

where

$$M_R(\xi,\tau)=\begin{cases}2\varepsilon\bar{R}(\tau)\xi & \text{for } \xi<\frac{1}{2},\\ 2\varepsilon\bar{R}(\tau)(1-\xi) & \text{for } \xi\geqslant\frac{1}{2}\end{cases} \tag{7}$$

and

$$M_\mu(\xi,\tau)=-\frac{1}{12}\alpha^2\sum_{j=1}^{\infty}\frac{1}{j^2}\ddot{q}_{(j)}(\tau)\sin j\pi\xi, \tag{8}$$

where $\bar{R}(\tau)$ is the interaction force $R(t)$, normalized by the static load $(m_t+m_s)g$ and α is the speed parameter [7].

Fig. 2 shows DAF results corresponding to the spring–dashpot model of Fig. 1. This more elaborate model confirms Brady's finding [7,8] that there is an increasing series of velocities that result in DAF peaks of increasing magnitude.

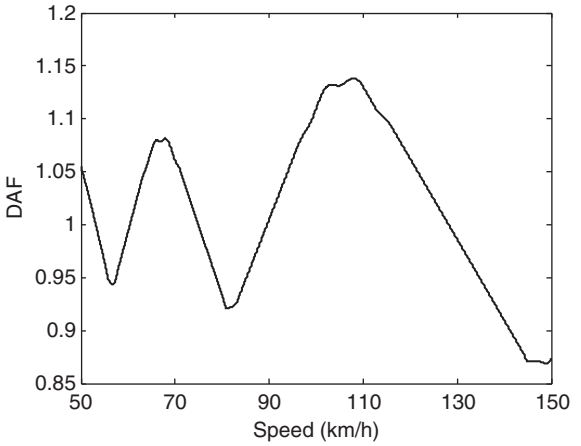

Fig. 2. DAF versus vehicle speed for model of Fig. 1 (smooth profile).

3. The effect of roughness on dynamic amplification

Many indicators of pavement surface evenness have been developed since the 1960s. The most popular parameters are the IRI [28–30], which was developed and recommended by the World Bank to evaluate pavement roughness, and the power spectral density (PSD). The PSD function, given by Yang and Lin [31], provides a method of modeling a random road surface. While they are widely used as measures of roughness, PSD and IRI are not good predictors of bridge dynamic response, despite the significant influence of road profile on bridge dynamics. Fig. 3 shows the response of the bridge to the vehicle on two different road surfaces, each with the same IRI (2.78 m/km) and PSD. The difference in responses shows that IRI and PSD are insufficient to predict dynamic bridge amplification and its relationship with vehicle speed.

In numerical simulations, the authors found that the effect of surface profile on bridge dynamic amplification is strongly dependent on the positions of the particular changes in profile (ramps) which neither IRI nor PSD measure. Using the simplified bridge–vehicle interaction model described in Section 2, this paper introduces a new way to explain the effect of the bridge surface profile on dynamic amplification.

3.1. The effect of the ramp

A unit ramp is defined as a ramp of 1 mm height over a 100 mm length as illustrated in Fig. 4. The ramp location is defined by reference to the start point of its 100 mm length. This segment length was chosen based on the assumption that only frequencies of less than 10 cycles per meter (wavelengths of greater than 100 mm) are significant [15].

In order to analyze the effect of the ramp on bridge dynamic amplification, a unit ramp is incorporated into an otherwise smooth bridge surface at all possible locations. The DAF for a range of speeds and unit ramp locations, DAF^{unit}, is illustrated in Fig. 5(a). The DAF for this bridge and vehicle can be seen to be primarily affected by vehicle speed with the critical dynamic amplification occurring at about 105 km/h. This is unsurprising given the small ramp magnitude and Fig. 5(a) in fact gives very similar results to those of Fig. 2 which corresponds to a smooth profile. The differences between Figs. 5(a) and 2 are illustrated in Fig. 5(b). The influence of speed has clearly not been completely removed in this figure, indicating an interaction between ramp location and speed.

Fig. 6 illustrates the DAF due to a ramp of magnitude 10 mm (over a 100 mm length). The speed is still clearly important and the same critical speeds are evident. However, for a ramp of this magnitude, the location is also important and it can be seen that, for some locations (e.g., $0.23 \times$ length), the DAF can be low at a critical speed such as 105 km/h. The ramp has no influence on the maximum total moment when it occurs in the right half of the bridge. When the vehicle arrives at that point, the maximum has already occurred.

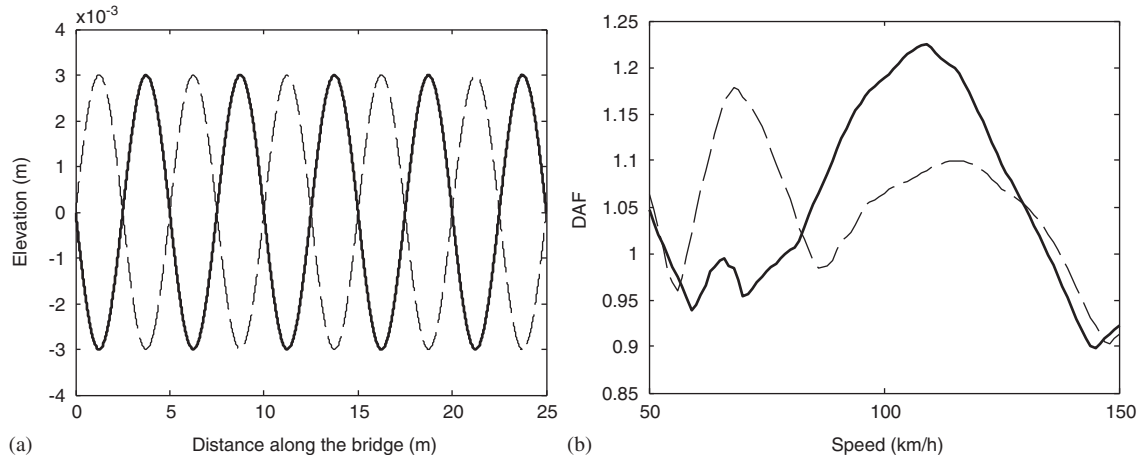

Fig. 3. Effect of two bridge surface profiles with identical IRI: (a) elevation of the two profiles, (b) DAF versus speed for the profiles in (a) —— case 1; ----- case 2.

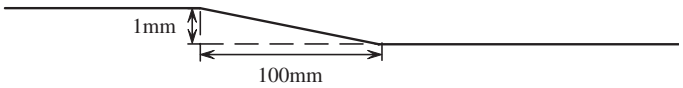

Fig. 4. Definition of positive unit ramp.

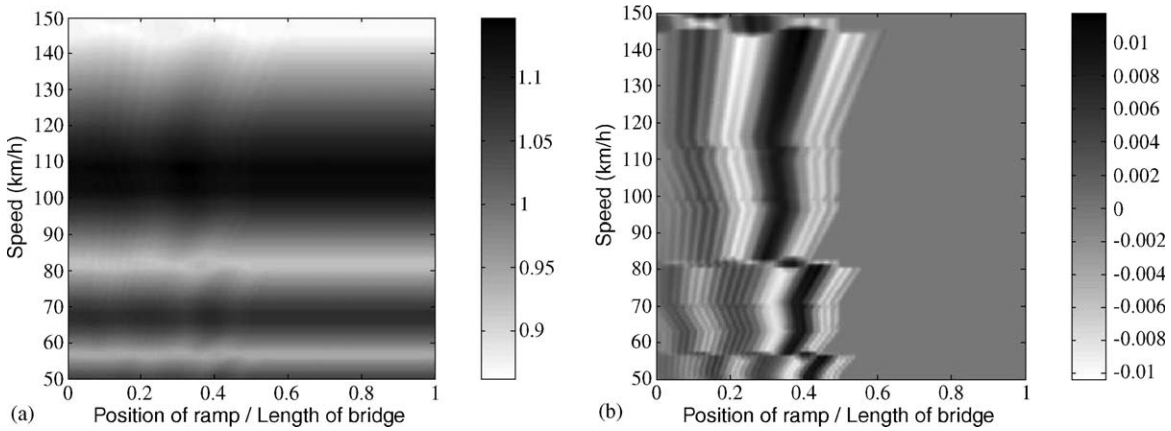

Fig. 5. DAF due to a positive unit ramp: (a) DAF for a unit ramp on an otherwise smooth profile (= DAF^{unit}), (b) difference in DAF between unit ramp and smooth profile (no ramp).

The authors have found that linear scaling of Fig. 5(b) is possible in the range of 1–10 with good accuracy, i.e., Fig. 6(b) can be very well approximated by scaling Fig. 5(b) by ten. The implication is that the maximum DAF due to a single ramp is almost linearly related to the height of a ramp for heights up to 10 mm. This phenomenon is mathematically explained in the next section.

3.2. The principle of ramp superposition

Bending moment is caused by bridge inertial forces and vehicle forces as presented in Eq. (6). The vehicle forces depend on the relative displacement of the tire spring which is related to the road irregularities and

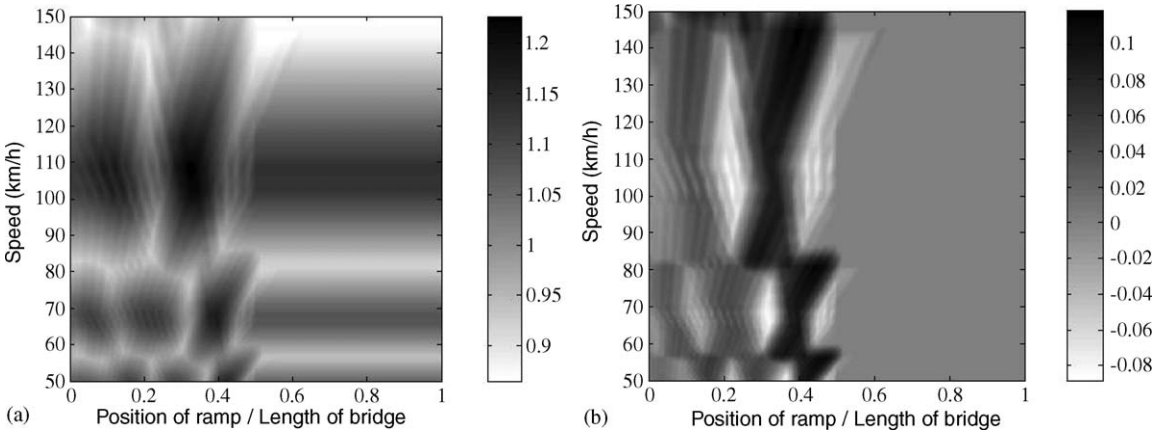

Fig. 6. DAF due to positive ramp of 10 mm: (a) DAF for a 10 mm ramp on an otherwise smooth profile, (b) difference in DAF between 10 mm ramp and smooth profile (no ramp).

beam deflection. However, for short spans the deflection of the beam has been shown to be small relative to the irregularities in the profile and the resulting interaction forces can be assumed negligible ($v(x_1, t) \approx 0$ in Eq. (2)) [21].

A single-degree-of-freedom undamped sprung mass is used in this section to demonstrate the principle of ramp superposition that is applied to the bending moment due to vehicle forces. The equation of motion of this single-degree-of-freedom system due to the unit ramp is given by

$$m_t \frac{\mathrm{d}^2 y_t(t)}{\mathrm{d}t^2} + K_t y_t(t) = \begin{cases} 0.001 K_t\left(\frac{t}{0.1/c}\right), & 0 \leqslant t \leqslant (0.1/c), \\ 0.001 K_t, & t \geqslant (0.1/c). \end{cases} \tag{9}$$

For initial conditions $y_t(0) = 0$ and $\mathrm{d}y_t(0)/\mathrm{d}t = 0$, the solution of this differential equation of second order is

$$y_t(t) = \begin{cases} 0.001\left[\left(\frac{t}{0.1/c}\right) - \left(\frac{1}{\omega_n 0.1/c}\right)\sin(\omega_n t)\right], & 0 \leqslant t \leqslant (0.1/c), \\ 0.001\left[1 + \left(\frac{1}{\omega_n 0.1/c}\right)[\sin(\omega_n(t - 0.1/c)) - \sin(\omega_n t)]\right], & t \geqslant (0.1/c), \end{cases} \tag{10}$$

where $\omega_n = \sqrt{K_t/m_t}$.

For another profile defined by a single unit ramp located 0.1 m from the ramp above (i.e., starting where the ramp described above ends), the solution is given by

$$y_t(t) = \begin{cases} 0, & 0 \leqslant t \leqslant (0.1/c), \\ 0.001\left[\left(\frac{t-0.1/c}{0.1/c}\right) - \left(\frac{1}{\omega_n 0.1/c}\right)\sin(\omega_n(t - 0.1/c))\right], & (0.1/c) \leqslant t \leqslant 2(0.1/c), \\ 0.001\left[1 + \left(\frac{1}{\omega_n 0.1/c}\right)[\sin(\omega_n(t - 2 \times 0.1/c)) - \sin(\omega_n(t - 0.1/c))]\right], & t \geqslant 2(0.1/c). \end{cases} \tag{11}$$

Next a profile is considered which has two adjacent ramps, each 0.1 m long, with heights H_1 downhill followed by H_2 uphill. The equation of motion is given by

$$m_t \frac{\mathrm{d}^2 y_t(t)}{\mathrm{d}t^2} + K_t y_t(t) = \begin{cases} K_t H_1\left(\frac{t}{0.1/c}\right), & 0 \leqslant t \leqslant (0.1/c), \\ K_t H_1 - K_t H_2\left(\frac{(t-0.1/c)}{0.1/c}\right), & (0.1/c) \leqslant t \leqslant 2 \times (0.1/c), \\ K_t H_1 - K_t H_2, & t \geqslant 2 \times (0.1/c). \end{cases} \tag{12}$$

For initial conditions $y_t(0) = 0$ and $dy_t(0)/dt = 0$, the solution of Eq. (12) is

$$y_t(t) = \begin{cases} H_1 \times 0.001\left[\left(\frac{t}{0.1/c}\right) - \left(\frac{1}{\omega_n 0.1/c}\right)\sin(\omega_n t)\right], & 0 \leqslant t \leqslant (0.1/c), \\ H_1 \times 0.001\left[1 + \left(\frac{1}{\omega_n 0.1/c}\right)[\sin(\omega_n(t-0.1/c)) - \sin(\omega_n t)]\right], & \\ \quad -H_2 \times 0.001\left[\left(\frac{t-0.1/c}{0.1/c}\right) - \left(\frac{1}{\omega_n 0.1/c}\right)\sin(\omega_n(t-0.1/c))\right], & (0.1/c) \leqslant t \leqslant 2(0.1/c), \\ H_1 \times 0.001\left[1 + \left(\frac{1}{\omega_n 0.1/c}\right)[\sin(\omega_n(t-0.1/c)) - \sin(\omega_n t)]\right], & \\ -H_2 \times 0.001\left[1 + \left(\frac{1}{\omega_n 0.1/c}\right)[\sin(\omega_n(t-2\times 0.1/c)) - \sin(\omega_n(t-0.1/c))]\right], & t \geqslant 2(0.1/c). \end{cases} \tag{13}$$

It can be seen that the solution given by Eq. (13) corresponds to the solution given by Eq. (10) multiplied by H_1 minus the solution given by Eq. (11) multiplied by H_2. In other words, it is possible to scale and superpose the dynamic responses of the bridge to individual ramps. A small inaccuracy in this superposition process arises from the discretization process and assumption of negligible bridge deflection.

3.3. The estimation of DAF

It is proposed in this paper to estimate DAF by simple superposition of the effects of all individual ramps that together make up the surface profile. The estimate is referred to as the dynamic amplification estimate (DAE). The ramp scale factor of the profile at successive 100 mm intervals, $s(i)$, is defined by

$$s(i) = \frac{[r(x_{i+1}) - r(x_i)]}{h_u}, \tag{14}$$

where $r(x_i)$ is the road surface elevation at position x_i on the bridge and h_u is the height of the unit ramp. The DAE is defined as the DAF for a smooth profile plus the sum, for all locations, of the DAF due to a unit ramp at that location, scaled by the magnitude of the ramp:

$$\mathrm{DAE}(c) = \mathrm{DAF}^{\mathrm{smooth}}(c) + \sum_{i=1}^{N}[\mathrm{DAF}^{\mathrm{unit}}(c,i) - \mathrm{DAF}^{\mathrm{smooth}}(c)] \times s(i), \tag{15}$$

where $\mathrm{DAF}^{\mathrm{smooth}}$ is the DAF for a smooth profile (Fig. 2), $\mathrm{DAF}^{\mathrm{unit}}$ is the DAF for a unit (1 mm) ramp (Fig. 5(a)) and N is the number of ramps in the profile (discretized at 100 mm intervals).

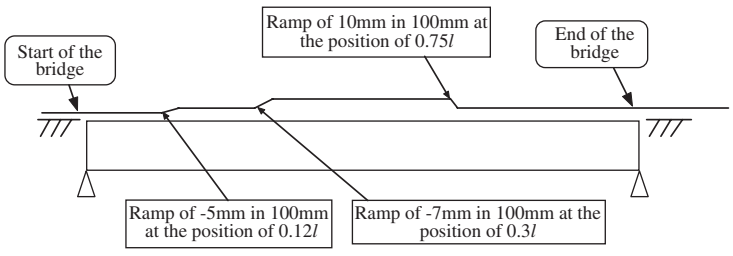

Fig. 7. Illustration of DAE concept.

Example. The DAE is required for a vehicle traveling at 110 km/h on the simple profile illustrated in Fig. 7 over a bridge of length l.

The DAE is found by adding the DAFs due to:

- a smooth surface (1.1302, found in Fig. 2)
- a unit ramp at $0.12l$ multiplied by -5 (0.00433 multiplied by -5, found in Fig. 5(b))
- a unit ramp at $0.3l$ multiplied by -7 (0.006031 multiplied by -7, found in Fig. 5(b))
- a unit ramp at $0.75l$ multiplied by 10 (0, found in Fig. 5(b))

The resulting DAE value for 110 km/h is 1.0663. The exact DAF as found by numerical simulation for this profile is 1.0656 implying an error of only 0.07%.

4. Validation

The accuracy of the DAE as an estimator of DAF is tested for three bridge spans, eight surface profiles and speeds in the range of 50–150 km/h. The eight profiles, all classified as 'good' according to the ISO standard, are illustrated in Fig. 8(a). The first six are typical of profiles measured on highways of good quality. The last two are artificial and are designed to generate extremes of DAF.

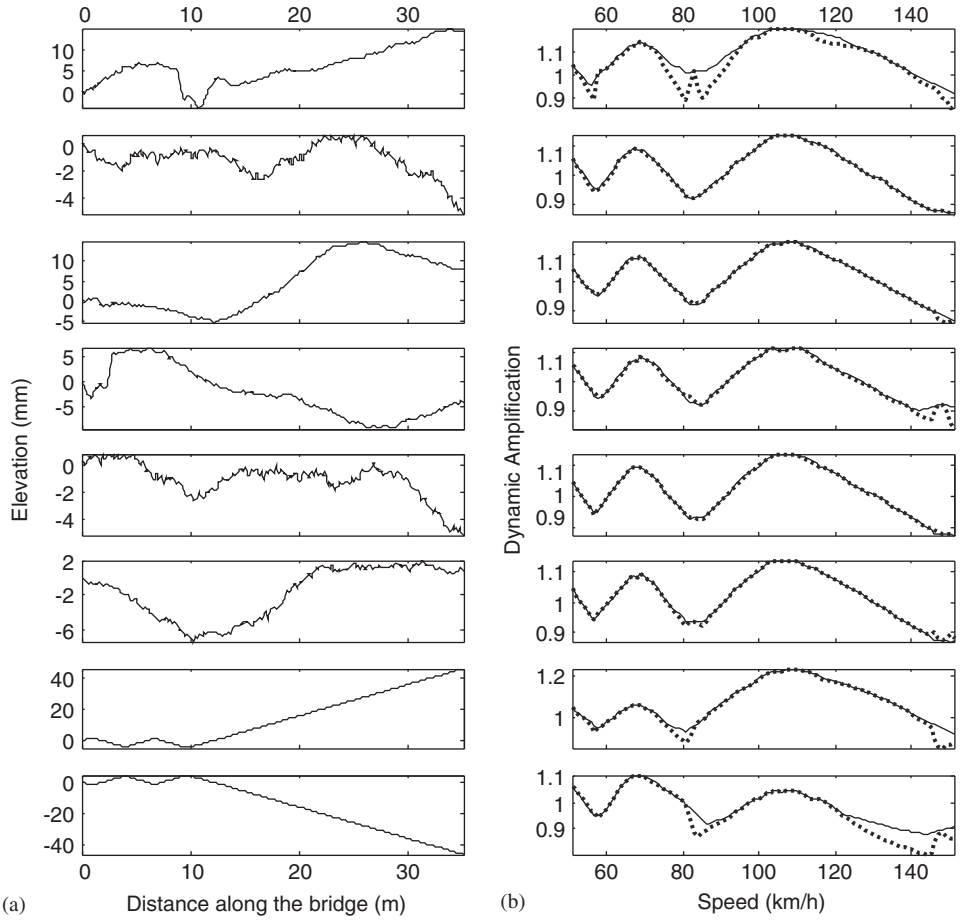

Fig. 8. Surface profiles for all bridges and comparison of DAF with DAE for 25 m bridge with vehicle initially in equilibrium and vertically stationary: (a) — eight road profiles, (b) — DAF (solid) and DAE (dotted) for the corresponding road profile.

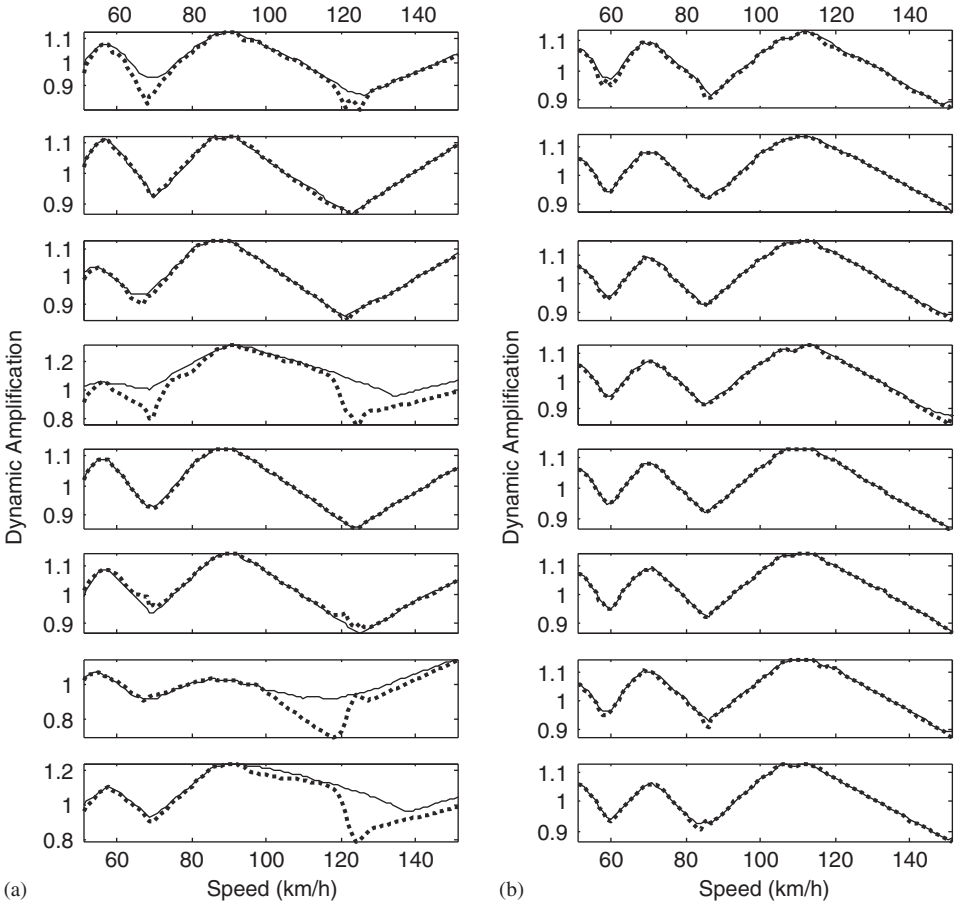

Fig. 9. Comparison of DAF (solid) with DAE (dotted) on (a) 15 m bridge and (b) 35 m bridge. Vehicle initially in equilibrium and vertically stationary.

Fig. 8(b) shows DAE and DAF for a wide range of speed for all eight profiles on the 25 m bridge. The initial condition is a vehicle in equilibrium with zero vertical velocity at the start of the bridge. The match between DAE and the DAF is very good, particularly for the real profiles where the speed is more significant than the profile. Where there are significant differences such as in the first profile, they correspond to velocities for which the DAF is not maximum. This is to be expected as maximum DAF tends to occur when the peak dynamic response coincides with the peak static response. In such situations, the DAE whose main source of error arises from differences in the locations of the peaks will be accurate. In all eight cases shown in Fig. 8(b), there is an excellent match in the maximum values of DAF/DAE.

Figs. 9(a) and (b) provide comparisons of DAF and DAE for 15 and 35 m bridges, respectively. For the 15 m span, a solid section was assumed for the calculation of mass per meter and second moment of area. For the 35 m span, beam and slab construction was assumed with super-Y precast beams [24,25]. The comparison of DAF with DAE can be seen to be good for all 8 profiles (Fig. 8(a)) for both bridge spans.

In all of the above analysis, the vehicle is assumed to have zero vertical velocity and acceleration at the time it arrives on the bridge. An alternative initial condition will affect the total bending moment in the bridge and hence the DAF and DAE. Thus, graphs such as Figs. 2 and 5 are only valid for the initial condition assumed. The accuracy of the DAE for an alternative set of initial conditions is illustrated in Fig. 11. For this analysis of the 25 m bridge, the vehicle is passed over a 200 m approach span (Fig. 10). It can be seen that, while DAF has changed due to the change in the initial conditions, the match between DAF and DAE is still good for all eight profiles. (Fig. 11)

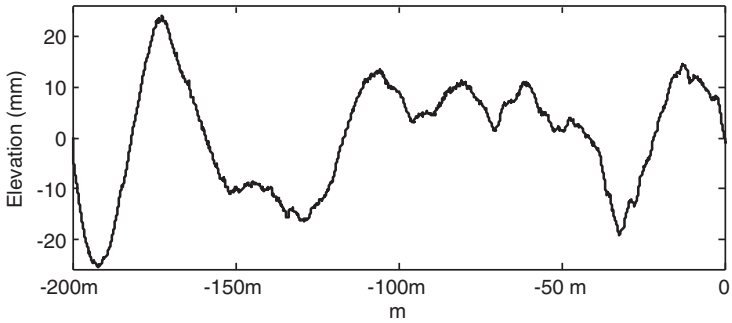

Fig. 10. Approach span profile.

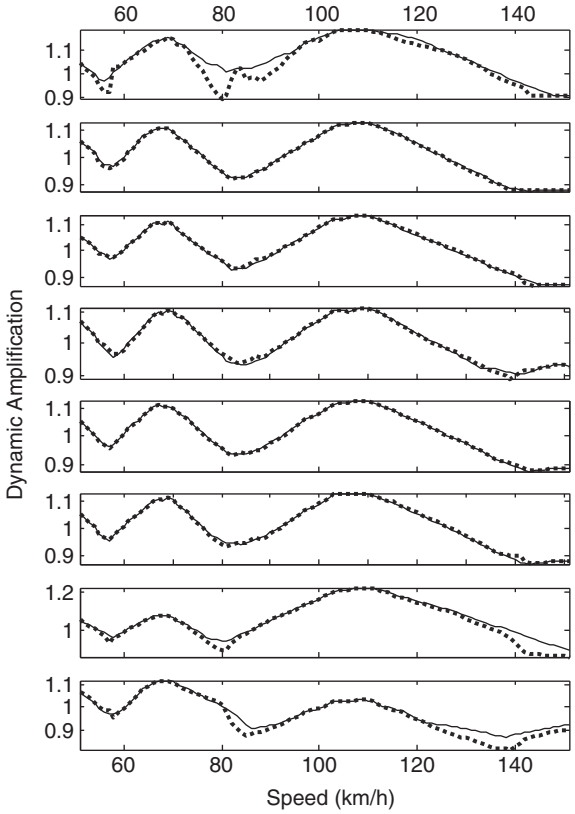

Fig. 11. Comparison of DAF (solid) with DAE (dotted) for the 8 profiles of Fig. 8(a). 25 m bridge with approach span and vehicle in motion on arrival at bridge.

5. Discussion

A simplified approximate method, DAE, is introduced to determine the influence of the road profile on bridge dynamics. It is based on the discretization of the road profile into a series of individual ramps and the superposition of the bridge responses to the passage of the vehicle over each individual ramp. DAE is shown to provide accurate DAFs when vehicle dynamics are small, i.e., for good road profiles and small bridge deflections relative to road irregularities.

DAE is intended to be used by Bridge Engineers who are seeking a measure of the extent to which the road profile will affect the stresses on a bridge. The road profile is processed through Eq. (15), which requires prior knowledge of the following bridge responses: (a) bridge response due to the vehicle under study running over a

smooth profile, DAF^{smooth} (i.e., Fig. 2) and (b) bridge responses due to the vehicle under study crossing a unit ramp located at different points before and on the bridge, DAF^{unit} (i.e., Fig. 5). Taking into account these two figures, it is possible to analyze the influence of any 'good' road profile without the need to solve the differential equations of motion each time the road profile changes.

The results are only valid for the vehicle model (and the parameter values) assumed in their derivation. While different initial conditions create different unit responses to those presented in Figs. 2 and 5, the road profile in the approach (and hence the initial conditions at the start of the bridge) can be taken into account by extending the DAF^{unit} figure to allow for ramps located prior to the bridge. Section 4 shows that maximum DAFs can still be predicted with good levels of accuracy.

In the same way as for the quarter-car model, the response of a multi-axle vehicle can be shown to be found by superposition of the unit responses to individual ramps but these unit responses are specific to the vehicle configuration and mechanical properties used. Nevertheless, the authors believe that the principle of ramp superposition is an important finding for assessing the critical locations where road irregularities have a significant effect on bridge dynamics.

6. Conclusion

A quarter-car vehicle model on a Bernoulli–Euler beam is used to investigate the influence of surface profile on the dynamic amplification of bending moment. For good surface profiles, the dynamic amplification due to a ramp is found to be approximately scaleable, i.e., for ramps of up to 10 mm over a 100 mm length, the dynamic amplification is well approximated by scaling the effect of a unit ramp and adding the effect of speed on a smooth profile. The interaction between speed and profile can also be seen.

A DAE is proposed as an indicator of the DAF. The DAE is easy to calculate and does not require the solution of differential equations when a new profile is considered. It involves a simple superposition of the effect of speed with the effect of each of the ramps that make up the profile. For a wide range of bridge spans, road profiles, speeds and initial conditions, the DAE is shown to be a good estimator of DAF, particularly for the peak values corresponding to critical speeds. The DAE concept has considerable potential as an assessment tool of the 'bridge friendliness' of surface profiles or as the basis for a 'bridge friendly' truck suspension system. With relatively little calculation, this approach makes it possible to accurately estimate peak DAF and determine the influence of surface profile on dynamic amplification. It also provides valuable insight into the road profile characteristics that influence amplification. The location of ramps is shown to be particularly important with adjacent ramps having the potential to be beneficial and detrimental.

References

[1] European Committee for Standardisation, *Eurocode 1: Basis of design and actions on structures—Part 3: traffic loads on bridges*, ENV 1991-3, 1991.
[2] DIVINE Programme, OECD, Dynamic interaction of heavy vehicles with roads and bridges, *DIVINE Concluding Conference*, Ottawa, Canada, 1997.
[3] M. Olsson, On the fundamental moving load problem, *Journal of Sound and Vibration* 154 (2) (1991) 299–307.
[4] C. Liu, D. Huang, T.L. Wang, Analytical dynamic impact study based on correlated road roughness, *Computers and Structures* 80 (2002) 1639–1650.
[5] S.P. Brady, E.J. OBrien, The effect of vehicle velocity on the dynamic amplification of two vehicles crossing a simply supported bridge, *Journal of Bridge Engineering, ASCE*, 2006, in press.
[6] M.F. Green, D. Cebon, D.J. Cole, Effects of vehicle suspension design on dynamics of highway bridges, *Journal of Structural Engineering, ASCE* 121 (2) (1995) 272–282.
[7] L. Frýba, *Vibration of Solids and Structures Under Moving Loads*, Noordhoff International Publishing, Groningen, The Netherlands, 1971.
[8] S. P. Brady, E.J. OBrien, A. Žnidarič, The effect of vehicle velocity on the dynamic amplification of a vehicle crossing a simply supported bridge, *Journal of Bridge Engineering, ASCE*, 2006, in press.
[9] D.H. Huang, T.L. Wang, M. Shahawy, Impact studies of multigirder concrete bridges, *Journal of Structural Engineering, ASCE* 119 (8) (1992) 2387–2402.
[10] X.Q. Zhu, S.S. Law, Dynamic load on continuous multi-lane bridge deck from moving vehicles, *Journal of Sound and Vibration* 251 (4) (2002) 697–716.

[11] G. Michaltsos, D. Sophianoplulos, A.N. Kounadis, The effect of a moving mass and other parameters on the dynamic response of a simply supported beam, *Journal of Sound and Vibration* 191 (3) (1995) 357–362.
[12] D. Karnopp, M.J. Crosby, R.A. Harwood, Vibration control using semi-active force generators, *Transactions of ASME, Journal of Engineering for Industry* 96 (1997) 619–626.
[13] D. Cebon, *Handbook of Vehicle– Road Interaction*, Swets & Zeitlinger, 1999.
[14] M. Valášek, M. Novák, Z. Šika, O. Vachlín, Extended ground-hook-new concept of semi-active control of truck's suspension, *Vehicle System Dynamics* 27 (1997) 289–303.
[15] O. Coussy, M. Said, J.P. Van Hoove, The influence of random surface irregularities on the dynamic response of bridges under suspended moving loads, *Journal of Sound and Vibration* 130 (2) (1989) 313–320.
[16] J.W. Kou, J.T. Dewolf, Vibration behavior of continuous span highway bridge-influencing variables, *Journal of Structural Engineering, ASCE* 123 (3) (1997) 333–344.
[17] X. Lei, N.A. Noda, Analyses of dynamic response of vehicle and track coupling system with random irregularity of track vertical profile, *Journal of Sound and Vibration* 258 (1) (2002) 147–165.
[18] P.K. Chatterjee, T.K. Datta, C.S. Surana, Vibration of continuous bridges under moving vehicles, *Journal of Sound and Vibration* 169 (5) (1994) 619–632.
[19] G.T. Michaltsos, Parameters affecting the dynamic response of light (steel) bridges, *Facta Universitatis, Series Mechanics, Automatic Control and Robotics* 2 (10) (2000) 1203–1218.
[20] A.V. Pesterev, L.A. Bergman, C.A. Tan, A novel approach to the calculation of pothole-induced contact forces in MDOF vehicle models, *Journal of Sound and Vibration* 275 (1–2) (2004) 127–149.
[21] A.V. Pesterev, L.A. Bergman, C.A. Tan, B. Yang, Assessing tire forces due to roadway unevenness by the pothole dynamic amplification factor method, *Journal of Sound and Vibration* 279 (3–5) (2005) 817–841.
[22] G.T. Michaltsos, T.G. Konstantakopoulos, Dynamic response of a bridge with surface deck irregularities, *Journal of Vibration and Control* 6 (2000) 667–689.
[23] A. González, Development of Accurate Methods of Weighing Trucks in Motion, Ph.D. Thesis, Department of Civil Engineering, Trinity College, Dublin, Ireland, 2001.
[24] H.P.J. Taylor, L.A. Clark, C.C. Banks, The Y-beam: a replacement for the M-beam in beam and slab bridge decks, *The Structural Engineer* 68 (23) (1990) 459–465.
[25] H.P.J. Taylor, The precast concrete bridge beam: the first 50 years, *The Structural Engineer* 76 (21) (1998) 407–414.
[26] S.S. Law, X.Q. Zhu, Bridge dynamic responses due to road surface roughness and braking of vehicle, *Journal of Sound and Vibration* 282 (3–5) (2005) 805–830.
[27] K. Chompooming, M. Yener, The influence of roadway surface irregularities and vehicle deceleration on bridge dynamics using the method of lines, *Journal of Sound and Vibration* 183 (4) (1995) 567–589.
[28] T.D. Gillespie, M.W. Sayers, L. Segel, *Calibration of Response-Type Pavement Roughness measuring Systems, National Cooperative Highway Research Program, Res. Rep. No. 228*, Transportation Research Board, National Research Council, Washington, DC, 1980.
[29] T.D. Gillespie, S.M. Karimihas, D. Cebon, M. Sayers, M.A. Nasim, W. Hansen, N. Ehsan, *Effects of Heavy-Vehicle Characteristics on Pavement Response and Performance, National Cooperative Highway Research Program, Res. Rep. No. 353*, Transportation Research Board, National Research Council, Washington, DC, 1993.
[30] J.A. Marcondes, M.B. Snyder, S.P. Singh, Predicting vertical acceleration in vehicles through pavement roughness, *Journal of Transport Engineering, ASCE* 118 (1) (1992) 33–49.
[31] Y.B. Yang, B.H. Lin, Vehicle–bridge analysis by dynamic condensation method, *Journal of Structural Engineering, ASCE* 121 (11) (1995) 1636–1643.